AJAPAS

African Journal of Advanced Pure and Applied Sciences (AJAPAS)

Online ISSN: 2957-644X
Volume 5, Issue 3, 2026
Page No: 116-121
Website: https://aaasjournals.com/index.php/ajapas/index

ISI 2025: 1.126 **SJIFactor 2024: 6.752** **معامل التأثير العربي: 1.62**

Cladding Process Design, Implementation & Simulation to Investigate the Quality of the Austenitic Stainless Steel Overlay on carbon steel Obtained by GMAW Process

Hassan Ali Saadawi [1*], Adel M. Daw [2], Aisa Abdulla Ighnegewa [3], Hesham R. Eshabani [4], Mohamed A. Saraj [5], Omaima M. Khubat [6]
[1,2,3,4,5,6] Advanced Occupational Center for Welding Technologies, Tripoli, Libya

تصميم وتنفيذ ومحاكاة عملية التكسية للتحقق من جودة تراكب الفولاذ المقاوم للصدأ الأوستنيتي على الصلب الكربوني باستخدام لحام القوس المستهلك والغازات الخاملة والنشطة

حسن علي السعداوي [1*]، عادل محمد ضو [2]، عيسى عبد الله اقنيجيوة [3]، شام رمضان الشعباني [4]، محمد اعمار السراج [5]، اميمة محمد الخباط [6]
[6,5,4,3,2,1] المركز الليبي المهني المتقدم لتقنيات اللحام، طرابلس، ليبيا

[*]Corresponding author: saadawi.hassan.74@gmail.com

Received: April 23, 2026	Accepted: July 04, 2026	Published: July 22, 2026

Abstract
In recent years, Weld cladding has attracted interest as a way to improve the surface property of equipment in corrosive environment by overlays of poor corrosion resistance materials with high corrosion resistance materials like stainless steel or nickel-based alloys. There are various problems effect clad quality such as residual stresses, distortion and bad dilution. In this study, the deposition of successive layer of austenitic stainless steel (ER 309L) on low carbon steel substrate were carried out using gas metal arc welding process by different deposition strategy. After experimental work, numerical simulation of cladding process based on Simufact welding software was done to estimate thermal cycle, residual stresses and distortion and compare the results with experimental output. The results show that the Relative percentage errors for the distortion derived from the simulations and the actual experimental data can reach 12.5% for one bead on plate strategy and 10.4 % for back strep strategy, for bead width the relative percentage error of one bead on plate strategy and back strep strategy is 11.8% and 10.2 % respectively.

Keywords: Weld cladding process, Gas metal arc welding, Simulation, Distortion.

الملخص
في السنوات الأخيرة، حظيت تقنية التكسية باللحام باهتمام متزايد كوسيلة لتحسين خصائص سطح المعدات في البيئات المسببة للتآكل، وذلك بتغطية مواد ذات مقاومة منخفضة للتآكل بمواد ذات مقاومة عالية للتآكل، مثل الفولاذ المقاوم للصدأ أو سبائك النيكل. من بين المشاكل على وتؤثر على جودة التكسية، الإجهادات المتبقية والتشوه. في هذه الدراسة، تم ترسيب طبقات متتالية من الفولاذ المقاوم للصدأ الأوستنيتي (ER 309L) على ركيزة من الفولاذ منخفض الكربون باستخدام لحام القوس المستهلك والغازات الخاملة والنشطة ، وذلك باتباع استراتيجيات ترسيب مختلفة. بعد التجارب العملية، أُجريت محاكاة عددية لعملية التكسية باستخدام برنامج Simufact لتقدير الدورة الحرارية والإجهادات المتبقية والتشوه، و من تم مقارنة نتائج المحاكاة بالنتائج العملية. تُظهر النتائج أن نسبة الخطأ للتشوه المستمد من عمليات المحاكاة و التجارب الفعلية يمكن أن تصل إلى 12.5% لاستراتيجية ترسيب طبقة واحدة و10.4% لاستراتيجية الشريط الخلفي، أما بالنسبة لعرض التكسية، فإن نسبة الخطأ النسبية لاستراتيجية ترسيب طبقة واحدة واستراتيجية الشريط الخلفي هي 11.8% و10.2% على التوالي.

الكلمات المفتاحية: التكسية باللحام، لحام القوس المستهلك و الغازات الخاملة، المحاكاة، التشوه.

1. Introduction

Materials that can be used in seawater and other harsh, corrosive conditions are expensive and this limits their application from an economic point of view. In such environments, resistance of wear and corrosion are required only at the surfaces of parts, which are always in contact with their surroundings [1]. Consequently, in order to provide a cost-effective solution for this technical difficulty, engineers are increasingly focusing on cladding or overlays of poor corrosion resistance materials with high corrosion resistance materials like stainless steel or nickel-based alloys [2,3].

Weld overlaying is the process of depositing a filler metal on a base metal (substrate) in order to provide the surface a desired characteristic that isn't inherent in the base metal. There are several types of weld overlays, including buildup alloys, buttering alloys, hardfacing materials, and weld claddings [4]. A base metal can be selected for cost or structural properties, and clad metal added for surface protection or some special property such as electrical conductivity [1]. Weld cladding is the process of covering one material with another, either internally or externally [5]. The principal cladding techniques include hot roll bonding, cold roll bonding, explosive bonding, centrifugal casting, brazing, and welding [4]. The weld cladding usually refers to application of a relatively thick layer (>3 mm) of weld metal for the purpose of providing a corrosion-resistant surface [4]. Weld cladding is usually performed using different types of arc welding like manual metal arc welding, gas tungsten arc welding and gas metal arc welding [4,5]. Among the processes employed for weld cladding, gas metal arc welding is the most commonly used cladding process. The advantages in using gas metal arc welding for cladding are: high reliability, all positional capability, ease of use, low cost, high productivity, suitability for all metals and high deposition rate [6,7,8]. All welding filler metals can also be used for cladding. Filler metals often vary from base metals in terms of composition and properties [9]. Various materials like nickel, cobalt, copper and manganese are used for weld cladding applications [9].

The cladded steel components are widely used in chemical, petroleum, and marine industries [5]. The cladding filler metal is usually an austenitic stainless steel or a nickel-base alloy [4]. Due to their high corrosion and oxidation resistance property, stainless steels are important materials that have been used widely in a variety of industries and environments. Austenitic stainless steels are a group of steels (300 series) that contain nominally 19 % chromium and 9 % nickel. Among the many 300 series stainless steels grades, AISI 309L stainless steel is extensively used as cladding filler metal [10]. The difference in the thermal expansion coefficient between the cladding material and the base metal results distortion of cladded part because of induced thermal stresses. The temperature history during the cladding process and the geometry of the cladded component, all affect the amount and distribution of the cladding residual stresses and distortion [1,11].

Analytical methods were mostly used to solve heat conduction problems prior to the advancement of computational science. However, these analytical solutions can only be applied to a limited number of simple geometries and boundary conditions, but for complex condition , analytical techniques are not valid. This problem can be solved with numerical methods [12]. For expensive materials such austenitic stainless steel, evaluating of thermal cycle, distortion and residual stresses through experimental cladding trials may not be suitable. As a result, simulation permits to evaluate the metallurgical and mechanical properties before introducing the process into real production [13,14,15].

Several researche papers discussed the cladding of carbon steeel by austenitic stainless steel. Sreeraj et al. [6] used full factorial design matrix for development of mathematical model to predict clad angle of austenitic stainless steel deposited by gas metal arc welding and find that This method is useful to get optimum clad angle. Yoganandh et al. [7] appleid The response surface methodology to estimate clad bead geometry for austenitic steel cladding, results were very close to the experimental results. Kannan et al. [8] found that the Artificial Neural Network (ANN) models can be used as an alternative tool for calculation of clad bead geometry of stainless steel cladding deposited by gas metal arc welding method. Venkateswara et al. [9] investigated the interface between high strength low alloy steel with austenitic stainless steel cladded by gas metal arc welding, the interface between the two steels was nearly flat. Purohit et al. [1] simulated submerged arc welding cladding process using finite element software ANSYS to predict heat distribution and residual stress. Same results have been reported by Siegele et al. [11] the resultes of numerical simulation of the submerged arc welding cladding process are in agreement with measurements with X-ray diffraction technique. In this work, numerical simulation was used to simulate the weld cladding process and predict the thermal cycle, distortion and residual stresses using a commercial software package, Simufact welding software [16], and compare the results with experimental output. Experimental and numerical simulation works have been carried out at the (Advanced Occupational Center for Welding Technologies) in Tajura, Tripoli, Libya.

2. Experimental Work

2.1 Materials

In this experimental work, two steels have been employed:

1- Low carbon steel plate (S235-SPM-sw) St 37 with the dimensions of 200 mm × 80 mm × 10 mm were used as substrates to carry out the experiments.
2- Austenitic stainless steel filler wire which was standardized as per SFA/AWS A5.9 : ER309L and EN ISO 14343-A:G 23 12 L, was used as the feedstock material in the experiments [17]. The chemical composition of ER309L filler material and low carbon steel S235-SPM-sw are shown in Table 1.

Table 1. Chemical composition of ER309L and St 37 [17].

Alloy /Wt.%	C	Mn	Si	N	Ni	Cr	Mo	Fe
ER309L	0.02	1.8	0.4	0.05	13.4	23.2	0.1	Bal.
S235-SPM-sw	0.15	0.491	0.073		0.03	0.001	0.008	Bal.

2.2 Equipment

The system used to perform cladding deposition is composed by the integration of two different systems:

- Welding system. In this work, the semi-automatic Miller MigMatic® S400iP gas metal arc welding machine was used as the weld cladding process.
- Three-axis movement system, the motion of the system should be easily controlled.

The power source and movement system used for the described experimental work in this section is shown in the Figure 1.

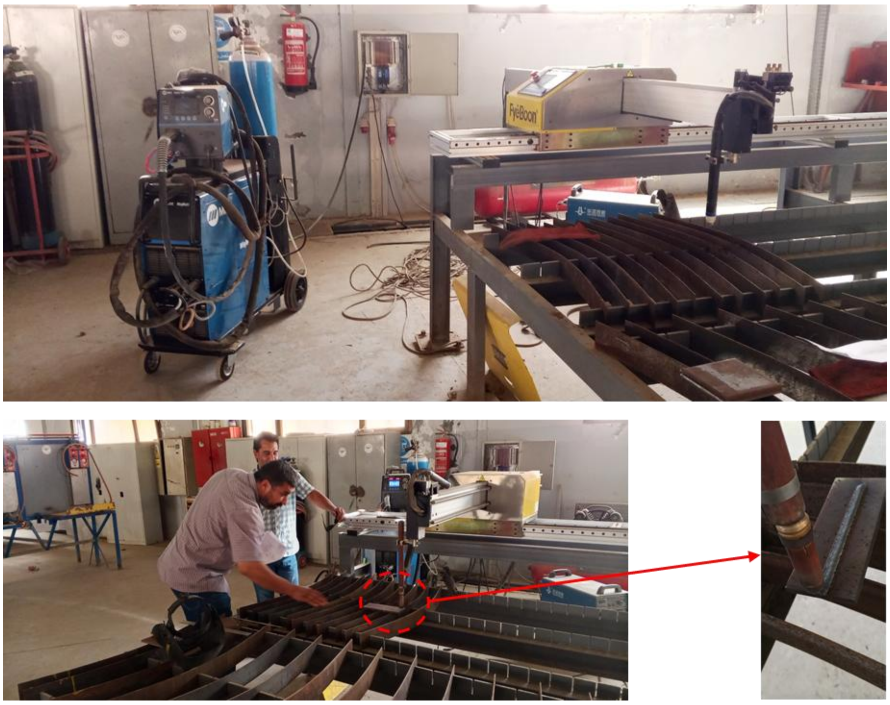

Figure 1. Power source and movement system.

2.3 Definition of Cladding Process Parameters

a series of cladding trial runs were conducted using gas metal arc welding power source based on the working range of the input parameters (welding current , welding voltage and welding speed), which chosen according to previous studies that covered weld cladding of stainless steel and ESAB welding filler Metal data book [6,7,8,17,18]. Weld clad quality was considered acceptable when the resulted beads were free from visual defects like macrocracking, excessive convexity and spatter and surface porosity. The best process parameters are presented in Table 2.

Table 2. Cladding parameters

Parameter	Setting
Welding process	GMAW
Welding position	PA (1G)
Average current	200 A
Average voltage	24 V
Welding speed	400 mm/min
Wire feed rate	5 m/min
Wire diameter	1.2 mm
Shielding gas flow rate	18 L/min
Contact tube distance	12 mm

2.4 Weld Cladding Procedure

Two carbon steel plates with the dimension 200 x 80 x 10 mm were used as substrates. The plates were cleaned to remove dirt and located at flat position. These plates were cladded using gas metal arc welding technique and reversed polarity between the wire electrode and substrate in all runs. ER309L austenitic stainless steel filler wire was used as cladding material. Two different strategies of cladding were used as following :

1. Clad-1 : One bead on plate strategy (see Figure 2-a.).
2. Clad-2 : Back strep strategy: the same direction of deposition (see Figure 3-a.). When a deposit run was completed, the torch back to the starting point of the next deposit in the form of single layer and 3 runs.

The employed cladding parameters were kept constant for all deposited layers as given in the Table 2. To protect the weld pool from atmospheric contamination a mixture of Ar + 2% O2 was used as shielding gas.

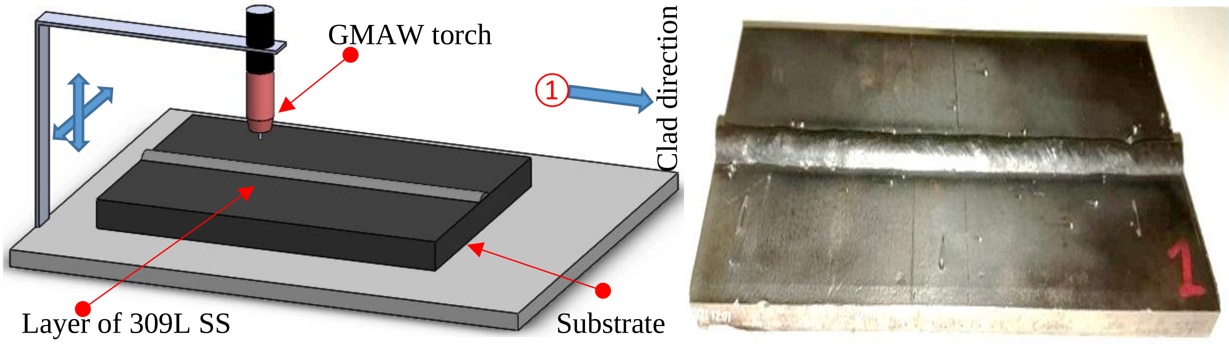

(a) (b)

Figure 2. (a) Clad-1 strategy , (b) Clad-1 appearance.

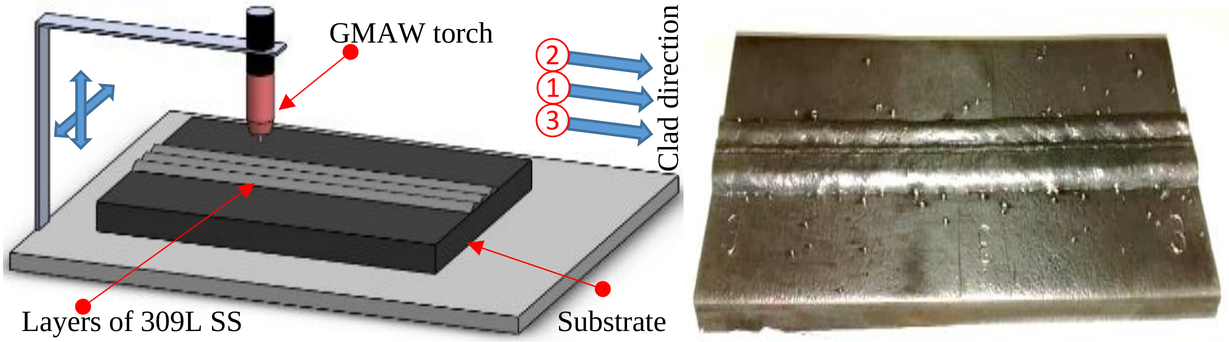

(a) (b)

Figure 3. (a) Clad-2 strategy , (b) Clad-2 appearance.

2.5 Integrity Assessment of the Cladded Beads

2.5.1 Appearance and Morphology

Deposited clads performed by gas metal arc welding were visually inspected to check surface imperfections. The cladding morphologies under different strategies of cladding were shown in Figure 2-b and Figure 3-b. The clads were continuous and the width of the beads were relatively uniform. No obvious pores, cracks and other defects were found on the surface of the clads.

2.5.2 Radiographic Examination

All cladded samples were inspected by X-ray radiographic examination according to ASTM E1742[19], and radiographs of Figure 4 were evaluated as per the requirements and definitions in ASME BPV Code Section IX [20]. The quality level employed for radiography was 2 % (2-2T using hole type IQI). The cladded parts were free of cracks and no lack of fusion or volumetric discontinuities were detected.

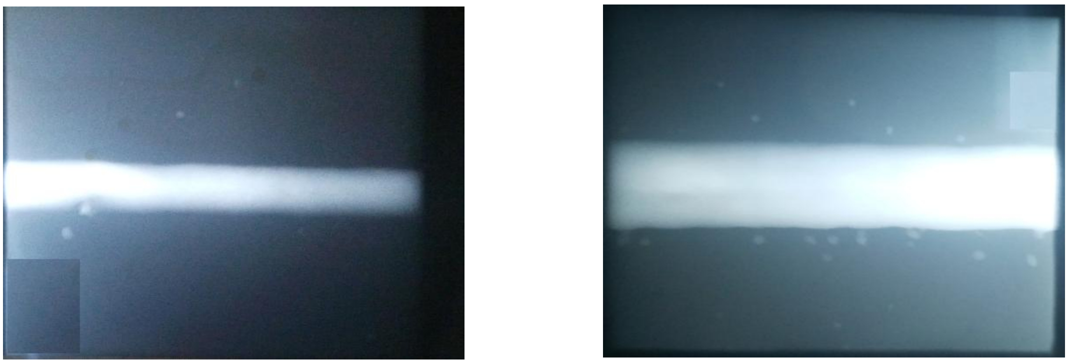

Figure 4. radiographic images of clad-1 and clad-2

2.5.3 Macroscopic Characterization

After visual and radiographic inspection, samples from transverse side of cladded parts were taken for macroscopic evaluation in order to check internal imperfections, as seen in Figure 5. This evaluation included measurement the macrosection of the clad bead. The sample were grinded and polished using 9, 6 and 1 µm colloidal alumina suspension, then etched by 5% Nital for 20 s at room temperature. All specimens were examined using HST Metallurgical Microscope Model: 402-AW. The macrosection of the cladded bead under different strategies of cladding were shown in Figure 6.

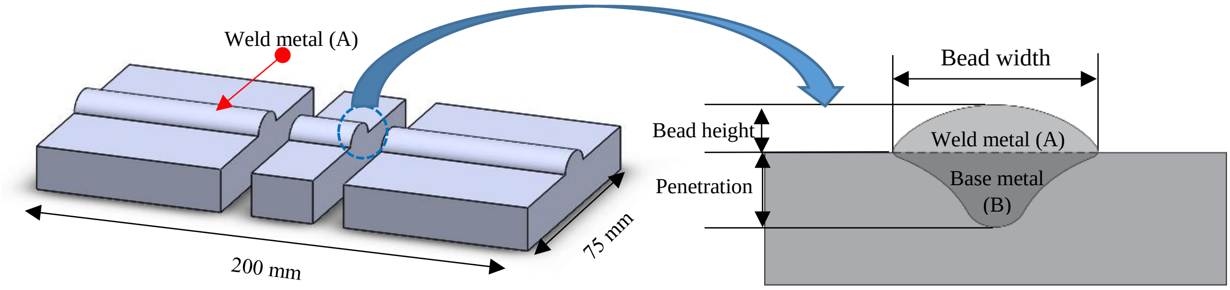

Figure 5. Macrosection sample

Clad-1 Clad-2

Figure 6. Macrosection images of clad-1 and clad-2

The macrosection and weld pool surface ripple markings images were taken using a high resolution scanning machine as illustrated in Figure 7 and Figure 8 respectively, and the dimensions were measured using the ImageJ® image processing software [21]. The clad bead dimensions are presented in Table 3.

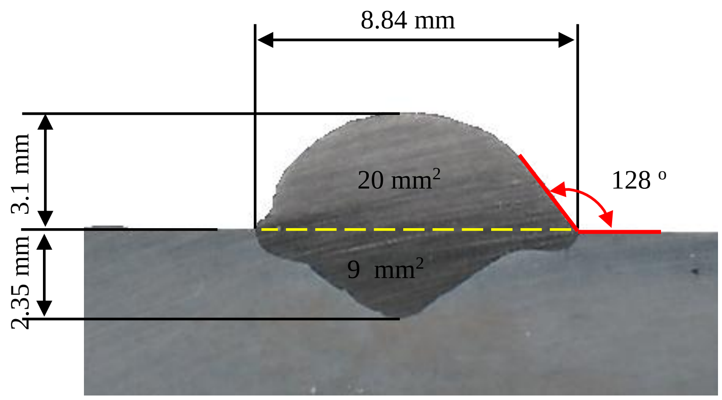

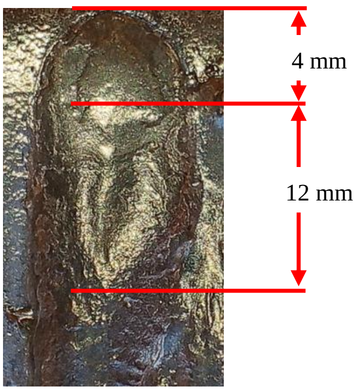

Figure 7. Macrosection images of clad-1 Figure 8. Weld pool surface

Table 3. The clad bead dimensions.

Measurements (mm)	Value
Bead width (b)	8.84
Bead height (h)	3.10
Penetration depth (P)	2.35
Front length (a_f)	4
rear length (a_r)	12
Area A	20
Area B	9

2.5.4 Dilution

Dilution is commonly expressed as the percentage of base metal that has been mixed with the weld metal [5]. When the value is greater than 10 it considered acceptable. Less than 10% refers to problem in bond integrity [4]. Dilution is calculated as follows:

$$\text{Dilution} = B/A+B \qquad (1)$$

Where B is the amount of base metal melted and A the amount of filler metal added see Figure 7.
Based on clad bead dimensions in Table 3 and equation (1) Dilution is calculated as:

$$\text{Dilution} = 9/20+9$$

Dilution = 31%

2.5.5 Convexity Index

Convexity index is an important factor used to evaluate the quality of the clad bead and expressed as the a ratio of clad bead height to clad bead width. [22,23]. According to several authors the ideal convexity index should be around 30% . [23].
From Table 3 the convexity index is :

$$\text{Convexity index} = \text{bead height} / \text{bead width} \qquad (2)$$

$$\text{Convexity index} = 3.1 / 8.84$$

Convexity index = 35%

2.5.6 Contact Angle

Contact angle defined by the angle between clad bead and base material. An angle of less than 90° resulted non-uniform bead shape deposition and voids between each cladding pass [24]. As illustrated in Figure 7 the contact angle is **(128°)**

2.6 Distortion

distortion is a dimensional changes of the cladded sample caused by heating and cooling cycles of cladding processes and, as seen in Figure 9, can be classified as:

− transverse shrinkage

− longitudinal shrinkage

− angular distortion , rotation of the structure around the cladding line and caused by nonuniform temperature distribution in the through-thickness direction; [25,26,27].

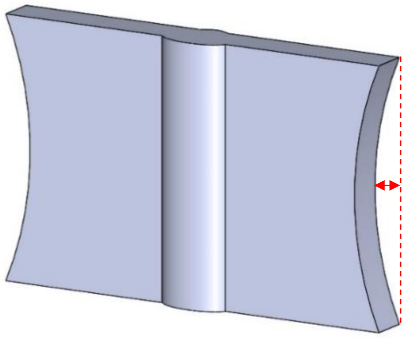

Transverse shrinkage

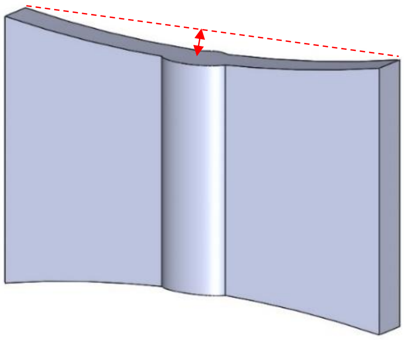

Longitudinal shrinkage

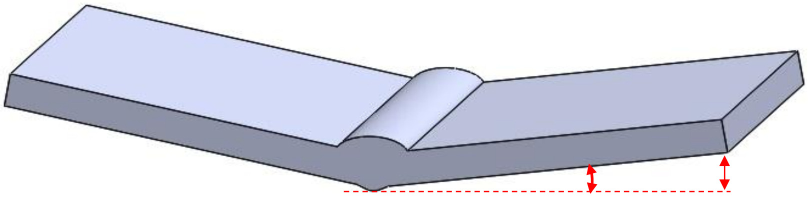

Angular distortion

Figure (9) Various types of cladding distortion. [26].

2.6.1 Measurement of Angular Distortion

Images from transverse side of cladded parts for two different strategies of cladding were taken using a high resolution scanning machine and angular distortion was measured using the ImageJ® image processing software [21]. As seen in Figure 10 and Figure 11, angular distortion of clad-1 and clad-2 are **0.49** and **1.724** respectively.

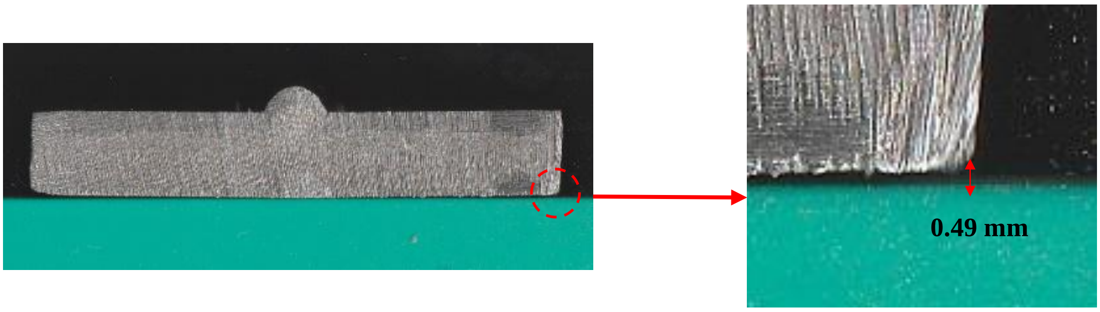

Figure 10. Angular distortion of clad-1.

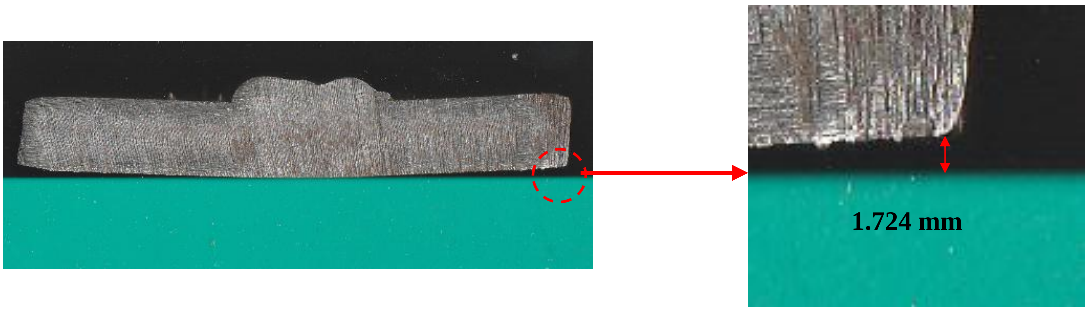

Figure 11. Angular distortion of clad-2.

3. Numerical Simulation Work

3.1 Numerical Modeling

The procedure of evaluate the thermal cycle, distortion and residual stresses through experimental cladding trials may not be suitable for expensive materials. Numerical modeling to simulate the cladding process is the best alternatives to these costly trials [13].

3.2 Software (Analytical Tool)

The research conducted involved the use of the Simufact welding software package developed by the MSC software company due to its flexibility in modeling and its capability in obtaining full field numerical solution. This software enables FEM-based simulation of cladding processes within a very wide range of heat sources like electric arc, laser beam and spot welding . Because of its design, the user interface is thought to be simple to use and understand. The software have a material library that contains a variety of pre-defined, frequently used materials that are categorized. Additionally, it is possible to make new materials, alter, and duplicate the ones that already exist. The software effectively predicts the heat distribution, distortions and residual stresses that happen during cladding, taking phase transformations into account and managing them in the component. This is one of the most crucial tasks [16]. The simulation results presented in this paper have been run with a desktop PC (Intel Core i3 and 12 GB RAM).

3.3 Numerical Simulation Model

In particular, the numerical simulation in this study is used to evolution of the angular distortion by simulate the cladding of austenitic stainless steel Grad (309L), the process simulation are designed in the form of two strategies described in section (3.4) using Simufact welding software. The material properties are given in Table 4 .

The geometrical size and schematic diagram of the computational domain are displayed Figure12. The model dimension is similar to real sample which used in experimental work also the same cladding parameters of experimental work was chosen to implement numerical simulation of cladding. Points T1, T2, T3 and T4 were selected to estimate the temperature, the distance between each point was 2 mm. Points D1, D2, D3 and D4 was selected to estimate the angular distortion.

Figure12 shows the finite element mesh model and the boundary conditions of cladding process which was used in the simulation. An eight node brick element is used to model the structures. There are 40 elements in the X direction and 5 elements in Z direction. In the Y direction, element meshes are fine near the clad centerline and coarser away from the clad centerline. This results in 5658 nodes and 4400 elements.

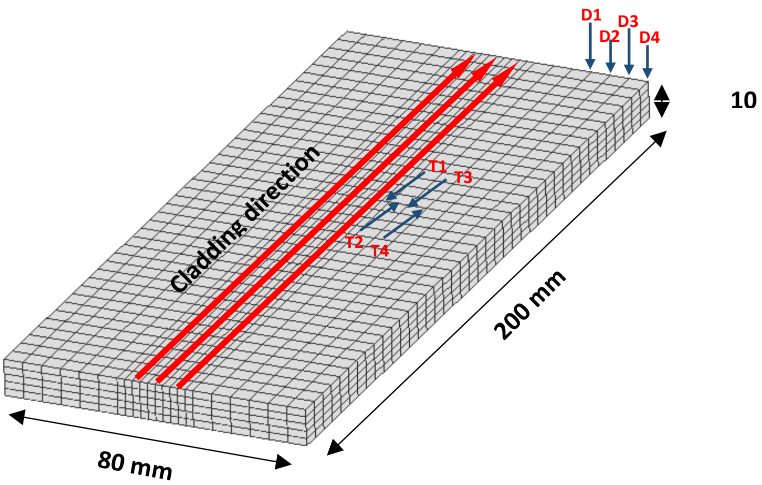

Figure 12. Geometrical size of the computational domain

Table 4. Austenitic stainless steel Grad (309L) properties.[28]

Property	Value	Unit
Thermal conductivity	14.5	W/(m.K)
Heat capacity at constant pressure	520	J/(kg.K)
Poisson's ratio of 309L at Room Temperature	0.29	--
Young's modulus 309L at Room Temperature	200×10^3	MPa
Density 309L at Room Temperature	8.03	g/m^3
Coefficient of thermal expansion 309L at Room Temperature	15.9×10^{-6}	1/K

3.4 Assumptions and Simplifications

For the cladding simulation, the following assumptions and simplifications have been made:

- isotropic and homogeneous material
- The cladding process is a heat conduction problem
- The initial temperature of the model is initially at 25°C.
- The fluid flow in the molten pool is neglected.
- The heat source is Goldak double ellipsoidal [29].
-

3.5 Heat Source Modeling and Boundary Conditions

It is necessary to define an appropriate heat source function based on the weld cladding process. In the international literature, there are essentially two options, which are depicted in Figure 13. The Goldak double ellipsoidal heat source is commonly applied for arc welding, whereas the 3D Gaussian heat source is applied to simulate electron beam or laser welding [30].

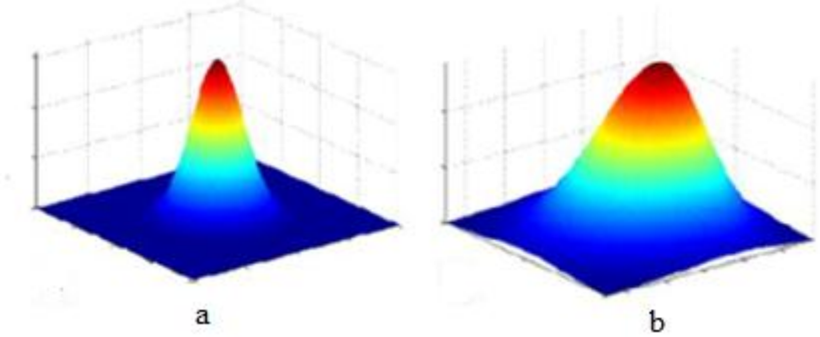

Figure 13. 3D heat sources a) Gaussian heat source , b) Goldak double ellipsoidal heat source.[30]

The Goldak double ellipsoidal heat source was used to simulate cladding as shown in Figure 14,

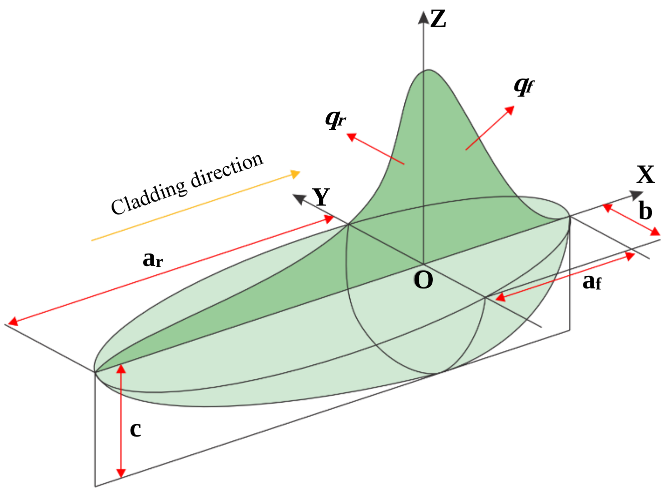

Figure 14. Goldak's double ellipsoidal heat source model [29]

In this model, the power density in front and rear of the arc center is described by Equations (3), (4) and (5) [29,30].

$$q_f(x,y,z) = \frac{6\sqrt{3}(f_f Q)}{a_f bc\pi\sqrt{\pi}}\, exp\left(-\frac{3x^2}{{a_f}^2} - \frac{3y^2}{b^2} - \frac{3z^2}{c^2}\right), \quad x \geq 0 \qquad (3)$$

$$q_r(x,y,z) = \frac{6\sqrt{3}(f_r Q)}{a_r bc\pi\sqrt{\pi}}\, exp\left(-\frac{3x^2}{{a_r}^2} - \frac{3y^2}{b^2} - \frac{3z^2}{c^2}\right), \quad x < 0 \qquad (4)$$

$$Q = \eta VI \qquad (5)$$

Where:
q_f and q_r are the heat flux on the front and the rear of the arc center.
a_f is the front length
a_r is the rear length;
b is the width of the heat source;
c is the depth of the heat source;
f_f and f_r are factors of the heat distributed in the front and rear of the heat source.
Q is the energy input while considering the factor of efficiency, calculated according to Equations. (5).
Equations (6) and (7), were used to calculate the boundary conditions of cooling between the workpiece and the environment through convection and radiation, respectively [29,30].

$$q_{con} = h(T - T_0) \qquad (6)$$

$$q_{rad} = \varepsilon\sigma\left(T^4 - {T_0}^4\right) \qquad (7)$$

where ε = 0.6 is the emissivity of ASS and h (10 $W/m^2.K$) is the natural convective heat transfer coefficient [31].

4. Results and Discussion

The main distortions to be compared in this study is the angular distortion. In order to compare the results of computation and experiment, the FE results are extracted from the measurement points which were used in experiments as shown in Figure12. The value of cladded bead dimensions and Goldak double-ellipsoidal heat source parameters are listed in table 3. The comparison of simulated and actual distortions, in two different strategies of cladding: one bead on plate strategy (Clad-1) and a three beads back strep strategy (Clad-2) have been considered.

4.1 Temperature Distribution

Figures 15, 16, and 17 show the temperature distribution plots and variation of the melt pool shape for start, mid and end of run. The total welding time was 120s and the maximum temperature rises up to 2600 ºC, which is higher than the melting temperature of steel.

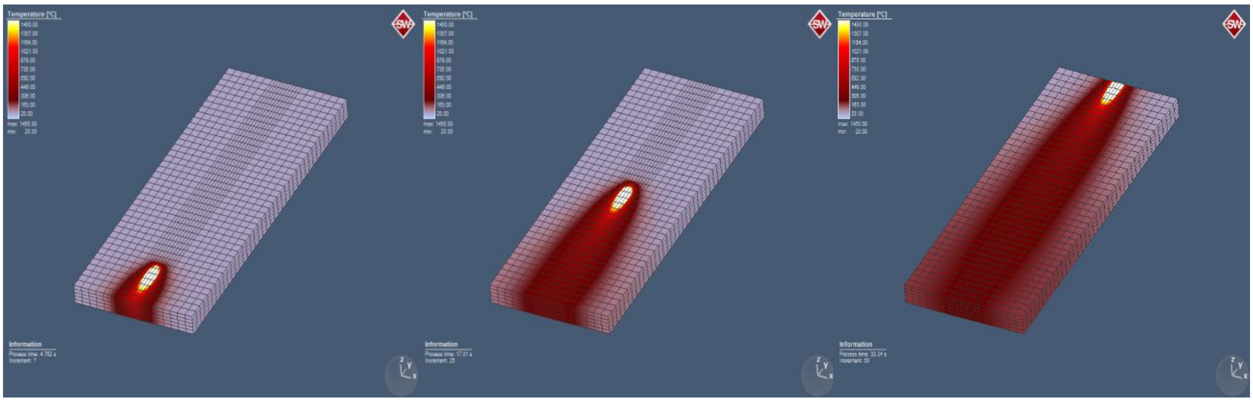

Figure**15.** Temperature distribution plots for start, mid and end of run

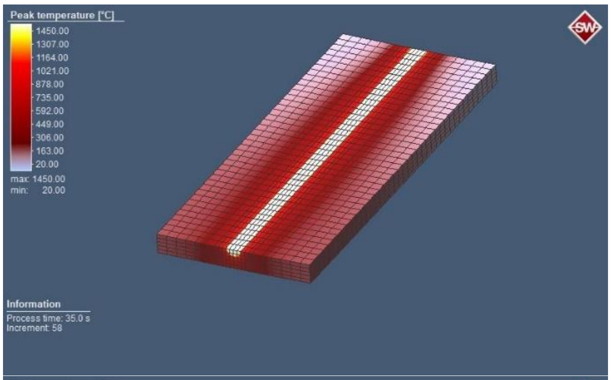

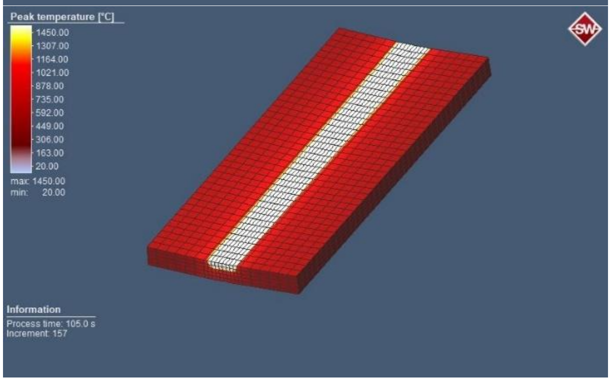

Figure16. Temperature distribution of Clad-1

Figure17. Temperature distribution Clad-2

4.2 Thermal Cycle Curve of Cladding

Figure 18 shows the thermal cycle curve at points with different distance from the center cladding line as seen in Figure 12. At T1, the temperature both increases and decrease very rapidly; and at T2, T3 and T4, the temperature curve changes more slightly, and the highest temperature also drops greatly.

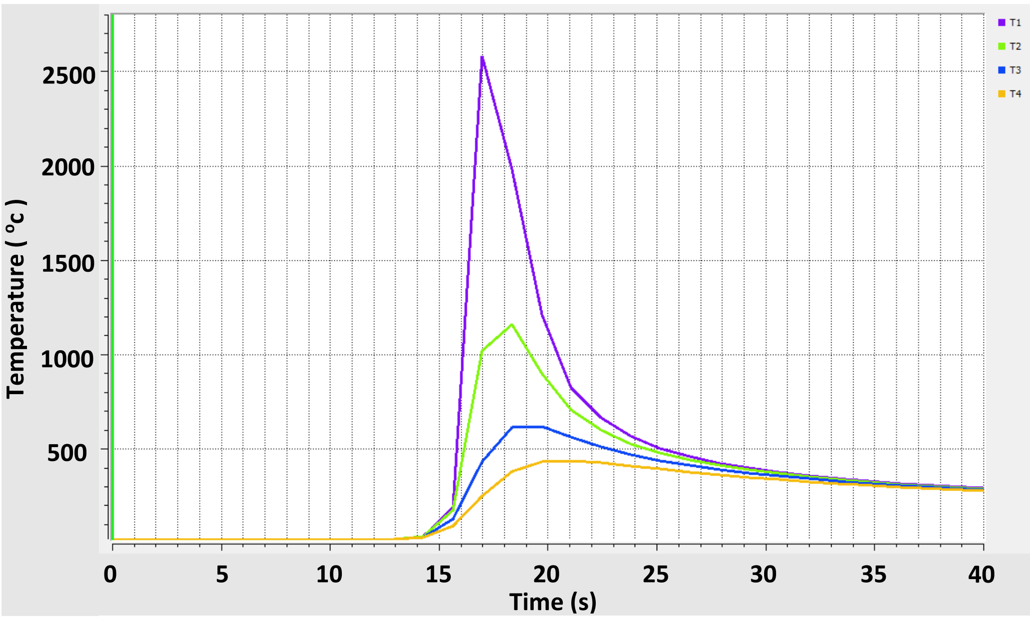

Figure18. Thermal cycle curve of clad-1

4.3 Temperature Field

The temperature field obtained from the simulation of two strategies can be seen in Figure 19 and Figure 20 . As seen in Figures, bead width of clad-1 and clad-2 are **7.9** mm and **18** mm respectively.

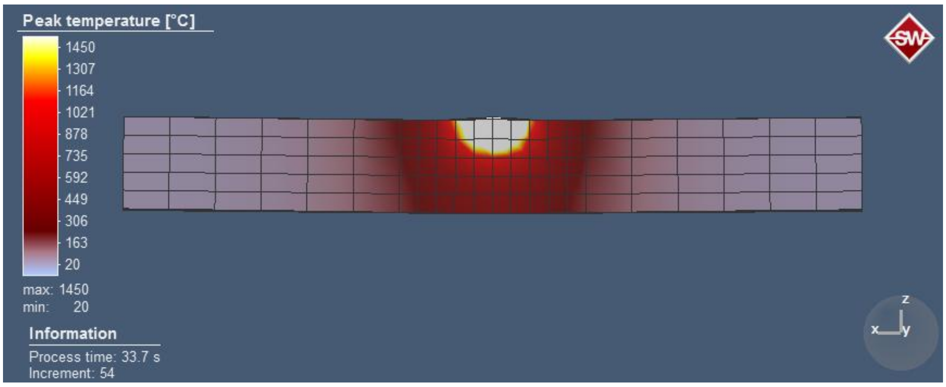

Figure **19.** Temperature field of clad-1

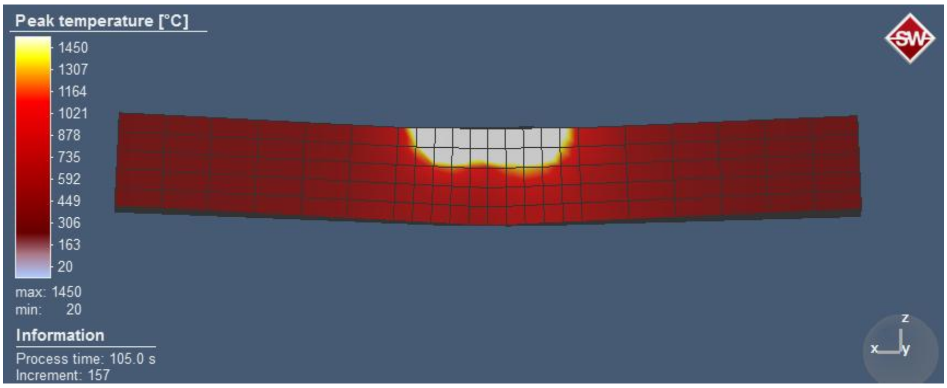

Figure **20.** Temperature field of clad-2

4.4 Cladding Distortions

During cladding process, parts are heated up to the melting temperature in cladding line then cooled slower than the heating process. For this reason uniform distribution of temperature is occur causes distortions of the part. The Angular distortion of cladded parts Clad-1and Clad-2 are shown in Figure 21 and Figure 22. Angular distortion occurred after cladding is approximately 0.56 mm in Clad-1 and 1.92 mm in Clad-2. Figure 23 and Figure 24 show the distortion in different time for two strategies.

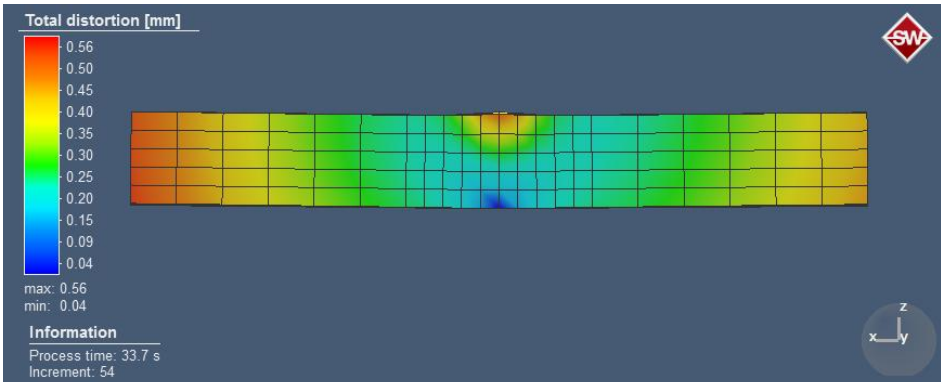

Figure **21.** Angular distortion of cladded parts Clad-1

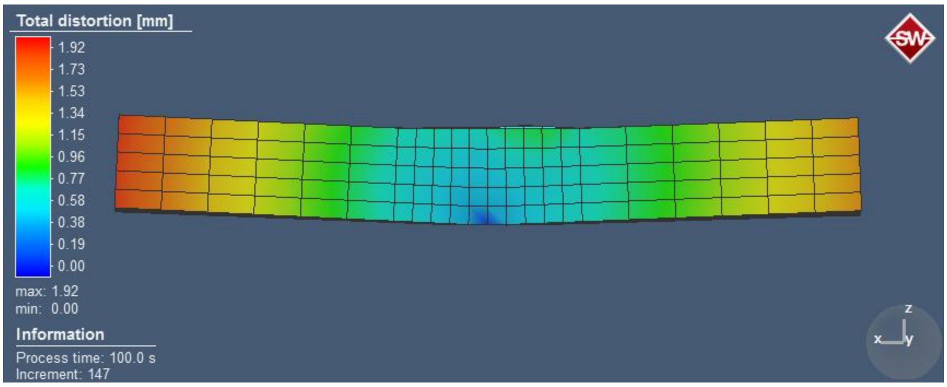

Figure **22.** Angular distortion of cladded parts Clad-2

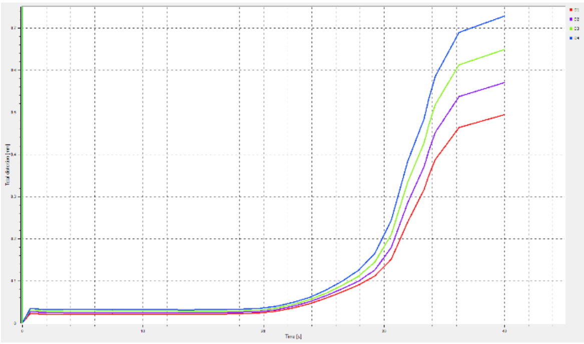

Figure **23.** distortion in different time for Clad-1

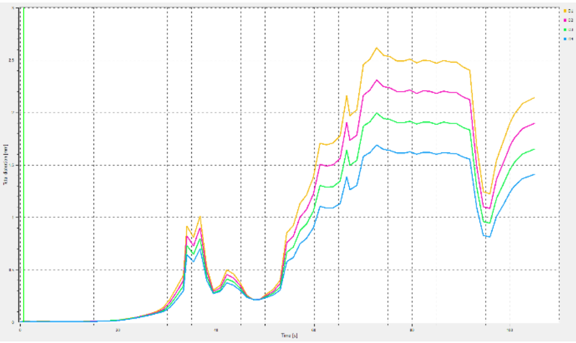

Figure **24.** distortion in different time for Clad-2

4.5 Residual Stress Evolution

The residual stress obtained from the simulation of clad-1 strategy can be seen in Figure **25 which** illustrated the numerical prediction contour of the residual stress. The maximum value of Stress is 266 N/mm^2 in cladding line.

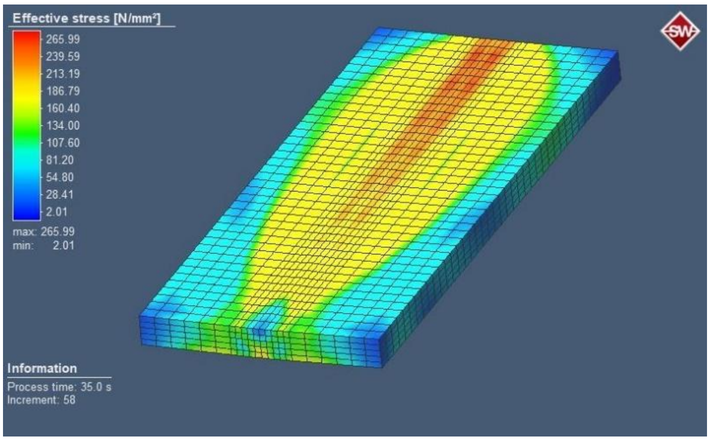

Figure 25. Numerical prediction contour of the residual stress

5. Model Validation

A comparison between the simulated and real results of two different strategies of cladding (clad-1 and clad-2) is used to give an experimental validation of the numerical model's effectiveness. The model's validity was confirmed by means of experimental data. The simulation findings were documented and compared with the experimental data, as indicated in Table 9.

Table 9. Experimental and simulation results.

Result	Experiment	Simulation	Error
Distortion of Clad-1 (mm)	0.49	0.56	12.5 %
Distortion of Clad-2 (mm)	1.72	1.92	10.4 %
Bead width of Clad-1 (mm)	8.84	7.90	11.8 %
Bead width of Clad-2 (mm)	19.83	18.00	10.2 %

Relative percentage errors for the Bead width derived from the models and the actual experimental data can reach 11.8% for Clac-1 and 10.2% for Clad-2, for distortion the relative percentage error of Clac-1and Clad-2 is 12.5% and 10.4 % respectively. These discrepancies are minor and to be expected given the model's assumptions about heat transport and the precision of the measurement instruments, leading to the conclusion that simufact welding software is a suitable method for simulating the cladding process.

6. Conclusions

The main conclusions that can be drawn from this study are as follows:

1. In the present study, we only studied the cladding distortion of the One bead on plate strategy (Clad-1) and Back strep strategy (Clad-2) , zig zag strategy not studied.
2. Relative percentage errors for the distortion derived from the simulations and the actual experimental data can reach 12.5% for Clac-1 and 10.4 % for Clad-2, for bead width the relative percentage error of Clac-1and Clad-2 is 11.8% and 10.2 % respectively.
3. The results show that the cladding temperature field, cladding macrosection shape and cladding distortions can be predicted by Simufact welding software. The predicted results are in good agreement with the experiment measurements.
4. As a result, numerical analysis makes it possible to significantly reduce prototyping costs and to consider a greater number of possible solutions without risking additional costs. This method also enables the analysis of difficult and expensive issues as regards necessary testing equipment.

ACKNOWLEDGMENT

The authors acknowledge the funding and support from the Libyan Advanced Occupational Centre for Welding Technologies.

Compliance with ethical standards

Disclosure of conflict of interest

The authors declare that they have no conflict of interest.

References

[1] Purohit, G. K., and Kalakesh Baligar. "Cladding process simulation and residual stress estimation using finite element coupled Field analysis." *International Journal of Engineering Research & Technology, Karnataka, India* 1, no. 8 (2012): 1-12.

[2] Alvarães, Camila Pereira, Francisco Carlos Albuquerque Madalena, Luís Felipe Guimarães de Souza, Jorge Carlos Ferreira Jorge, Leonardo Sales Araújo, and Matheus Campolina Mendes. "Performance of the INCONEL 625 alloy weld overlay obtained by FCAW process." *Matéria (Rio de Janeiro)* 24 (2019): e-12290.

[3] Rebelo Kornmeier, Joana, Maria José Marques, Weimin Gan, António Castanhola Batista, Sanjooram Paddea, and Altino Loureiro. "Quantification of residual stress relief by heat treatments in austenitic cladded layers." *Materials* 15, no. 4 (2022): 1364.

[4] J.R. Davis, Davis & Associates. "Stainless Steel Cladding and Weld Overlays" ASM International, 1994.

[5] Saha, Manas Kumar. "Gas metal arc weld cladding and its anti-corrosive performance-a brief review." *Athens Journal of Technology & Engineering* (2018).

[6] Sreeraj, P., T. Kannan, and S. Maji. "Prediction and optimization of stainless steel cladding deposited by GMAW process using response surface methodology, ANN and PSO." *Int. J. Eng. Sci* 3, no. 5 (2013): 30-41.

[7] Yoganandh, J., T. Kannan, S. P. Kumaresh Babu, and S. Natarajan. "Optimization of GMAW process parameters in austenitic stainless steel cladding using genetic algorithm based computational models." *Experimental Techniques* 37, no. 5 (2013): 48-58.

[8] Sreeraj, P., and T. Kannan. "Modelling and prediction of stainless steel clad bead geometry deposited by GMAW using regression and artificial neural network models." *Advances in Mechanical Engineering* 4 (2012): 237379.

[9] Rao, N. Venkateswara, G. Madhusudhan Reddy, and S. Nagarjuna. "Weld overlay cladding of high strength low alloy steel with austenitic stainless steel–structure and properties." *Materials & Design* 32, no. 4 (2011): 2496-2506.
[10] Saha, Saptarshi, Manidipto Mukherjee, and Tapan Kumar Pal. "Microstructure, texture, and mechanical property analysis of gas metal arc welded AISI 304 austenitic stainless steel." *Journal of Materials Engineering and Performance* 24, no. 3 (2015): 1125-1139.
[11] Siegele, Dieter, and Marcus Brand. "Numerical simulation of residual stresses due to cladding process." In *ASME Pressure Vessels and Piping Conference*, vol. 42843, pp. 1021-1025. 2007.
[12] Perret, William. *Welding simulation of complex automotive welded assembly-Possibilities and limits of the application of analytical temperature field solutions*. Bundesanstalt für Materialforschung und-prüfung (BAM), 2013.
[13] Dhinakaran, V., Suraj Khope, N. Siva Shanmugam, and K. Sankaranarayanasamy. "Numerical prediction of weld bead geometry in plasma arc welding of titanium sheets using COMSOL." In *Proceedings of the 2014 COMSOL Conference in Bangalore*, pp. 13-14. 2014.
[14] Roger, F., and A. Traidia. "Modeling Residual Stresses in Arc Welding." *Proceedings of the COMSOL* (2010).
[15] Kik, Tomasz. "Numerical analysis of MIG welding of butt joints in aluminium alloy." *Biuletyn Instytutu Spawalnictwa w Gliwicach* 58 (2014).
[16] Simufact engineering gmbh "Structural Welding Simulation" 2016.
[17] ESAB Team, "Welding Filler Metal Data book," ESAB, USA, 2016.
[18] Cui, Shuwan, Shuwen Pang, Dangqing Pang, Qin Zhang, and Zhiqing Zhang. "Numerical simulation and experimental investigation on 2205 duplex stainless steel K-TIG welded joint." *Metals* 11, no. 8 (2021): 1323.
[19] ASTM Subcommitte E28.04, ASTM E8, "Standard Practice for Radiographic Examination," American Society for Testing and Materials, USA, 2013.
[20] ASME Committe, "ASME Boiler and Pressure Vessel Code, New York:," The American Society of Mechanical Engineers, USA, 2011.
[21] W. Rasband, ImageJ, National Institutes of Health, Bethesda, Maryland, USA, 1997-2018.
[22] Prabhu, R., T. Alwarsamy, R. Ramakrishnan, and Parikshith S. Gargyan. "Development of mathematical model for prediction of convexity index in cladding by pulsed MIG welding process." *Procedia Materials Science* 5 (2014): 663-668.
[23] Moreno, J., H. Pinto, and J. Ávila. "Characterization of welding parameters and microstructure in a coating made with a tubular electrode of SAE EC410NiMo on a SAE 1020 steel substrate by FCAW process." In *Conference: 21st International Conference Materials, Methods & Technologies*. 2019.
[24] Pickin, Craig Graeme, Stewaret W. Williams, and M. Lunt. "Characterisation of the cold metal transfer (CMT) process and its application for low dilution cladding." *Journal of Materials Processing Technology* 211, no. 3 (2011): 496-502.
[25] Jilabi, Abdul Sameea Jasim Abdul Zehra. "Controlling angular distortion in manual metal arc welding of austenitic stainless steels using back-step technique." *Journal of University of Babylon for Engineering Sciences* 26, no. 2 (2018): 311-319.
[26] Artem, Pilipenko. "Computer simulation of residual stress and distortion of thick plates in multi-electrode submerged arc welding and their mitigation techniques." *Trondheim: Norwegian University of Science and Technology* (2001).
[27] Yükler, Ahmet İrfan, and Memduh Kurtulmus. "Angular distortion in butt arc welding." *International Journal of engineering science and application* 2, no. 4 (2018): 137-144.
[28] SLV Duisburg GmbH," The Welding Engineer´s Current Knowledge ",2000.
[29] Samad, Z., N. M. Nor, and E. R. I. Fauzi. "Thermo-mechanical simulation of temperature distribution and prediction of heat-affected zone size in MIG welding process on aluminium alloy EN AW 6082-T6." In *IOP Conference Series: Materials Science and Engineering*, vol. 530, no. 1, p. 012016. IOP Publishing, 2019.
[30] Dénes Kollár and Balázs Kövesdi" Numerical Simulation of Welding Process ", Budapest University of Technology and Economics/Department of Structural Engineering, Budapest, Hungary.
[31] M. T. Santos, P. V. Muterlle and G. C. Carvalho, "Emissivity Caracterization in Stainless Steels Alloys for Application in Hidroeletric Turbines," Applied Mechanics and Materials, vol. 719, pp. 3-12, 2015.

